Flexural resonance mechanism of thermal transport across graphene-SiO_2 interfaces

Zhun-Yong Ong,[1,a)] Bo Qiu,[2] Shanglong Xu,[2,3] Xiulin Ruan,[2] and Eric Pop[4,5]
[1]*Institute of High Performance Computing, A*STAR, Singapore, Singapore 138632*
[2]*School of Mechanical Engineering, Purdue University, West Lafayette, Indiana 47907, USA*
[3]*School of Mechanical, Electronic, and Industrial Engineering, University of Electronic Science and Technology of China, Chengdu 611731, China*
[4]*Department of Electrical Engineering, Stanford University, Stanford, California 94305, USA*
[5]*Department of Materials Science and Engineering, Stanford University, Stanford, California 94305, USA*

(Received 26 December 2017; accepted 27 February 2018; published online 19 March 2018)

Understanding the microscopic mechanism of heat dissipation at the dimensionally mismatched interface between a two-dimensional (2D) crystal and its substrate is crucial for the thermal management of devices based on 2D materials. Here, we study the lattice contribution to thermal (Kapitza) transport at graphene-SiO_2 interfaces using molecular dynamics (MD) simulations and non-equilibrium Green's functions (NEGF). We find that 78 percent of the Kapitza conductance is due to sub-20 THz flexural acoustic modes, and that a resonance mechanism dominates the interfacial phonon transport. MD and NEGF estimate the classical Kapitza conductance to be $h_K \approx 10$ to 16 MW K^{-1} m^{-2} at 300 K, respectively, consistent with existing experimental observations. Taking into account quantum mechanical corrections, this value is approximately 28% lower at 300 K. Our calculations also suggest that h_K scales as T^2 at low temperatures ($T < 100$ K) due to the linear frequency dependence of phonon transmission across the graphene-SiO_2 interface at low frequencies. Our study sheds light on the role of flexural acoustic phonons in heat dissipation from graphene to its substrate. *Published by AIP Publishing.* https://doi.org/10.1063/1.5020705

I. INTRODUCTION

Thermal coupling at dimensionally mismatched interfaces (e.g., between 2D graphene and 3D substrates) is an important area of study, with both fundamental and technological relevance. From a fundamental perspective, such thermal coupling is expected to be different from that between two 3D solids, particularly when flexural 2D modes or hybridized 2D-3D vibrational modes are involved. From an applied perspective, graphene electronics such as interconnects[1,2] and RF transistors[3,4] are expected to operate at high power density, where heat must be efficiently sunk into their contacts or substrates.[5,6] Heat dissipation is ultimately limited by the thermal conductivity of the graphene or nanoribbon channel[7,8] and the thermal conductance of the device interfaces. Thus, thermal management of such devices requires an understanding of how heat is transported within and between nanomaterials. In the case of single-layer graphene (SLG), thermal transport across its interface with the surrounding insulating dielectric (e.g., SiO_2) plays a vital role in dissipating the waste heat, given the large surface-to-volume ratio of such devices.

Interfacial heat transfer at the SLG-SiO_2 interface involves several physical processes. One of them is remote phonon scattering, in which graphene electrons are scattered by surface polar excitations.[9–12] Another major one is the lattice vibrational coupling between the SLG and the substrate. Given that graphene-based transistors are required to operate at different temperatures and charge carrier densities, it is important to know how the Kapitza conductance varies under these conditions. This, in turn, necessitates a clearer picture of the underlying heat transfer physics.

In this work, we carefully examine the lattice thermal conductance with an atomistic model of the SLG-SiO_2 interface. The contribution from remote phonon scattering has been studied in another publication by two of the authors of this study, ZYO and EP.[13] Here, we use a combination of molecular dynamics (MD) simulation and analytical techniques in order to reach a deeper and more complete understanding of lattice interfacial thermal transport. Already, there exist a number of excellent analytical approaches by Persson and co-workers to the problem of lattice interfacial thermal conduction in supported graphene.[14–16] However, they rely on the long wavelength approximation and do not account for the atomistic character of the interface or the contribution of non-flexural modes. Nonetheless, the insights from their models are valuable, and should be complemented by the results of atomistic simulations. Other simpler analytical models, such as the acoustic mismatch (AMM) and diffuse mismatch models (DMM),[17,18] cannot be applied in a straightforward manner to this structure since they assume the medium on either side of the interface to be semi-infinite. This is especially true for interfacial thermal transport in a dimensionally mismatched system such as SiO_2-supported SLG, where the 2D graphene flexural modes are coupled with the Rayleigh-like modes of the 3D substrate.

Lattice thermal transport across the graphene-substrate interface has also been studied using non-equilibrium molecular dynamics (NEMD) simulations.[19,20] However, such simulations do not incorporate low-temperature quantum effects and cannot reveal the contributions of the individual modes.

a)Email: ongzy@ihpc.a-star.edu.sg

In these studies, graphene was sandwiched between two media,[19,20] and this encasing of graphene modifies its flexural motion and consequently the thermal transport characteristics at the graphene interfaces.[21] In many experimental devices,[5,7,22] graphene is not covered, and we expect their heat transfer physics to be different for bare graphene.

Consequently, this study addresses lattice thermal transport across the SLG-SiO_2 interface in *uncovered*, SiO_2-supported SLG. We use different yet complementary methods to simulate thermal transport with an atomistic model of the uncovered SLG-SiO_2 interface. The Green-Kubo (GK) method in MD simulations gives us the classical linear transport coefficient with the anharmonic effects included. We also employ the spectral energy density (SED) method[23–26] to analyze the SLG atomic motions and compute the energy dissipation rate by individual phonon modes. The SED analysis shows a pattern of energy dissipation consistent with the flexural resonance mechanism proposed by Persson and co-workers.[14–16] A modified version of the non-equilibrium Green's function (NEGF) method is then used to explore low-temperature quantum effects and quantify the polarization dependence, allowing us to identify the dominant phonon modes in interfacial heat dissipation.

II. ATOMISTIC MODEL OF GRAPHENE/SILICON DIOXIDE INTERFACE

In all our atomistic simulations, we use the model of SiO_2-supported SLG shown in Fig. 1, which was also employed by two of the authors (BQ and XR) in Ref. 25. The dimensions are $4.4\,\text{nm} \times 4.3\,\text{nm} \times 1.6\,\text{nm}$ for length, width, and height, respectively. Periodic boundary conditions are applied in the in-plane (x-y) direction, while no restrictions are applied to SLG motion in the out-of-plane (z) direction. We choose SiO_2 as the substrate to be consistent with recent experiments.[5,7,22,27,28] The LAMMPS package[29] is used to perform all MD simulations (GK and SED), while the code General Lattice Utility Program (GULP)[30] is used to calculate the force constant matrix in the NEGF simulations.

We adopt the Tersoff potential parameters optimized by Lindsay and Broido[31] to model the C-C interaction in SLG. Interactions within SiO_2 are modeled using Tersoff potentials parameterized by Munetoh *el al.*[32] C-Si and C-O interactions are assumed to be of van der Waals (vdW) type, and modeled using the Lennard-Jones (LJ) potentials

$$V(r_{ij}) = 4\chi\epsilon\left[\left(\frac{\sigma}{r_{ij}}\right)^{12} - \left(\frac{\sigma}{r_{ij}}\right)^{6}\right], \tag{1}$$

with the parameters $\epsilon_{\text{C-Si}} = 8.909\,\text{meV}$, $\sigma_{\text{C-Si}} = 3.629\,\text{A}$, $\epsilon_{\text{C-O}} = 3.442\,\text{meV}$, and $\sigma_{\text{C-O}} = 3.275\,\text{A}$, where χ is a dimensionless scaling factor and r_{ij} is the interatomic distance between the i-th and j-th atoms. To determine the numerical value of χ, we compute ΔE, the difference between the areal energy of the uncoupled SLG and SiO_2 and that of the coupled SLG-SiO_2 system, for different values of χ. We assume that ΔE is equal to the areal adhesion energy, which experimentally[33] has been found to be $0.45\,\text{J/m}^2$. We find that the value $\chi = 2.341$ best approximates the empirical areal adhesion energy, and is used for the rest of the MD and NEGF simulations. We note that this extraction, in of itself, is a small but important advance uncovered in the course of this study ($\chi = 1$ corresponds to the basic vdW interaction used in Ref. 25).

Five independent simulation runs are performed and averaged for each case study to minimize the statistical fluctuations in the SiO_2 surface morphology. The temperatures at which we perform the MD simulations are below the Debye temperature of SLG ($\sim$2100 K),[8] and temperature quantum corrections (QC) have been performed in a similar fashion to previous works.[34]

III. SIMULATION RESULTS AND DISCUSSION

A. Molecular dynamics simulations

We first study the system with classical MD simulations. We compute the classical Kapitza conductance h_{GK} using the Green-Kubo method,[23,35,36] which we describe in more detail in Appendix A. The system is initially equilibrated at a constant temperature $T = 300\,\text{K}$ for 0.2 ns before it is allowed to equilibrate as a micro-canonical (NVE) ensemble for another 1.0 ns. The instantaneous interfacial heat flux Q is recorded at intervals of 5 fs over a period of 1 ns. h_{GK} is calculated from the formula

$$h_{GK} = \lim_{t\to\infty} h(t) = \lim_{t\to\infty} \frac{1}{Ak_BT^2}\int_0^t d\tau\,\langle Q(\tau)Q(0)\rangle, \tag{2}$$

where A and k_B are the interfacial area and the Boltzmann constant, respectively. The time auto-correlation integral of the interfacial heat flux $h(t)$ is shown in Fig. 2. We find that $h_{GK} = 9.8 \pm 3.1\ \text{MW K}^{-1}\text{m}^{-2}$. The Green-Kubo computation

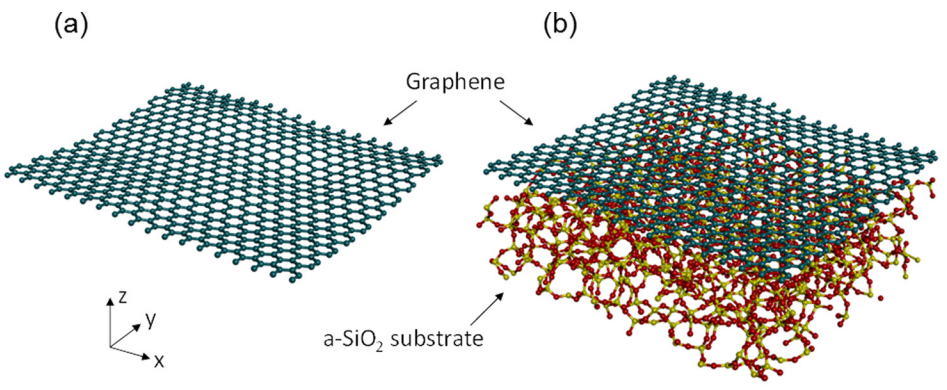

FIG. 1. Instantaneous geometry of both (a) suspended and (b) SiO_2-supported single-layer graphene (SLG). The SLG plane is parallel to the x-y plane, while the SLG out-of-plane direction aligns with z.

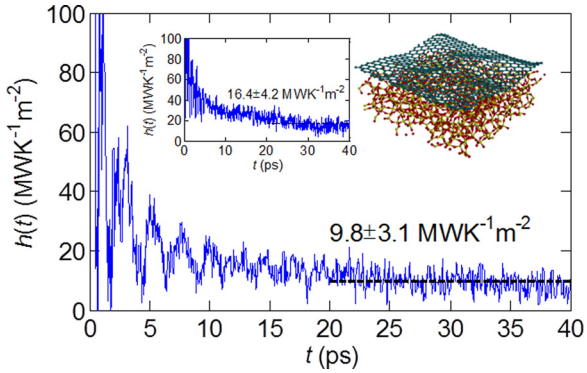

FIG. 2. Time auto-correlation function of the interfacial heat flux. The Green-Kubo Kapitza conductance (h_{GK}) is computed from its time integral. The inset shows the corresponding TACF for another sample which is more wrinkled and yields a larger h_{GK}.

is also repeated for a system domain that is 4 times larger (8.8 nm × 8.6 nm × 1.6 nm). The calculation yields $h_{GK} = 10.3 \pm 2.8$ MW $K^{-1}m^{-2}$, which is very close to the h_{GK} of the original domain size. This suggests that the domain size does not affect the Kapitza conductance significantly and agrees with the absence of any significant length effect on the Kapitza conductance seen in Ref. 37. It also implies that the long-wavelength phonon modes do not play a significant role in phonon transport across the interface, a conclusion reached independently in Ref. 21 where an elasticity-based model of the graphene-SiO_2 thermal boundary conductance is studied. We have also performed additional MD simulations with different SiO_2 surfaces, with the largest $h_{GK} = 16.4 \pm 4.2$ MW $K^{-1}m^{-2}$, consistent with additional simulation results obtained with the non-equilibrium MD method. This indicates that variation in the morphology of the surface can affect the thermal conductance of the interface.

Our Green-Kubo results are in good agreement with the simulated Kapitza conductance of the graphene-silicon carbide interface computed by Xu and Buehler[38] to be ~10 MW $K^{-1}m^{-2}$ at room temperature and low power density. They also showed that the Kapitza conductance increases substantially, from 12 to 43 MW $K^{-1}m^{-2}$, as the power density rises from 0.1 to 100 GW m^{-2}, and that the Kapitza conductance doubles to ~20 MW $K^{-1}m^{-2}$ when the temperature of the SLG reaches 1000 K. This increase in Kapitza conductance was posited to be due to the increased occupancy of high-frequency phonon modes at high temperatures. Using an indirect experimental approach, Freitag and co-workers[27] roughly estimated the Kapitza conductance of the SLG-SiO_2 interface to be around 25 MW $K^{-1}m^{-2}$ in SLG field-effect transistors during operation. A similar value (~25 MW $K^{-1}m^{-2}$) was reported by Mak and co-workers,[22] using an ultrafast pump-probe measurement technique applied to graphene samples on SiO_2. These experimental values are slightly higher than $h_{GK} = 10$ MW $K^{-1}m^{-2}$ we compute, although the experimental uncertainty is high, about 50%.[22] A plausible explanation for the discrepancy between the simulations and the experiments could be the high temperatures which the biased devices can reach (~1000 K in Ref. 27). Another source of discrepancy could also be electron-remote phonon scattering,[13] which is not captured in our MD simulations but estimated to be less than 5 MW $K^{-1}m^{-2}$ in SiO_2. Chen *et al.*[28] have also measured the Kapitza conductance of the SLG-SiO_2 interface in SiO_2-encased graphene, and found it to be between 80 and 180 MW $K^{-1}m^{-2}$, which is about one order of magnitude higher than our simulation results. This disparity may be due to the different nature of the interface in *encased* graphene, where the interfacial transport is between two three-dimensional solids which makes the transport efficient. Our SLG-SiO_2 interface is between 2D and 3D solids, and this dimensional mismatch makes interfacial transport inefficient. We have performed MD simulations of SiO_2-encased SLG and similarly found an order of magnitude increase in the Kapitza conductance, from ~50 to 100 MW $K^{-1}m^{-2}$, which will be the focus of a future publication.

We also increased the thickness of the SiO_2 substrate from 1.5 nm to 2.8 nm in order to see if the substrate depth affects the Kapitza conductance. The same simulation conditions for the earlier GK computation are imposed on the thicker (2.8 nm) SiO_2 substrate. We find that the thicker substrate yields a value of $h_{GK} = 9.7 \pm 2.9$ MW $K^{-1}m^{-2}$, close to that of the thinner 1.5 nm-thick substrate. This implies that the substrate depth is not a significant factor in our simulation. It reinforces the idea that the long-wavelength modes do not contribute much to interfacial thermal transport since the long-wavelength graphene phonon modes couple with the surface Rayleigh modes which scale as e^{qz}, where q is the wave vector and z the out-of-plane coordinate.[39]

Apart from facilitating interfacial thermal transport, the mechanical coupling between SLG and the SiO_2 substrate also reduces the lifetime of the SLG phonon modes through increased scattering.[25] Similar to Ref. 23 for carbon nanotubes, we now turn to relating the phonon lifetime reduction in SLG to the interfacial thermal transport by computing the SLG-SiO_2 phonon-phonon scattering rate γ_S. This scattering rate is obtained by taking the difference in the inverse phonon lifetime in MD simulations with a vibrating substrate (γ_{Vibr}) and with a frozen substrate (γ_{Froz})

$$\gamma_S = \gamma_{Vibr} - \gamma_{Froz}. \tag{3}$$

In the frozen substrate, there are no active substrate phonons and hence, no interfacial thermal transport. Thus, the *increase* in the inverse lifetime of the vibrating substrate is due to phonon-phonon scattering from interfacial thermal transport, γ_S.

We use the same equilibrium MD simulations for our GK simulations to compute γ_S. The atomistic configuration of the SLG-SiO_2 system used for the extraction of γ_S is identical to the one from which the first TBC value $h_{GK} = 9.8 \pm 3.1$ MW $K^{-1}m^{-2}$ is estimated using the GK method. Like in Ref. 25, the inverse lifetimes for modes in the first Brillouin zone (BZ) quadrant are computed. The computational details are given in Appendix B. The extracted γ_S for the three acoustic phonon branches [longitudinal (LA), in-plane transverse (TA), and flexural (ZA)], are shown in Figs. 3(a) to 3(c). The scattering rates of the optical phonon branches are not shown because their phonon-phonon scattering rates are much smaller than those of the acoustic phonons. Using the γ_S values and assuming that 50% of the phonon energy is lost per

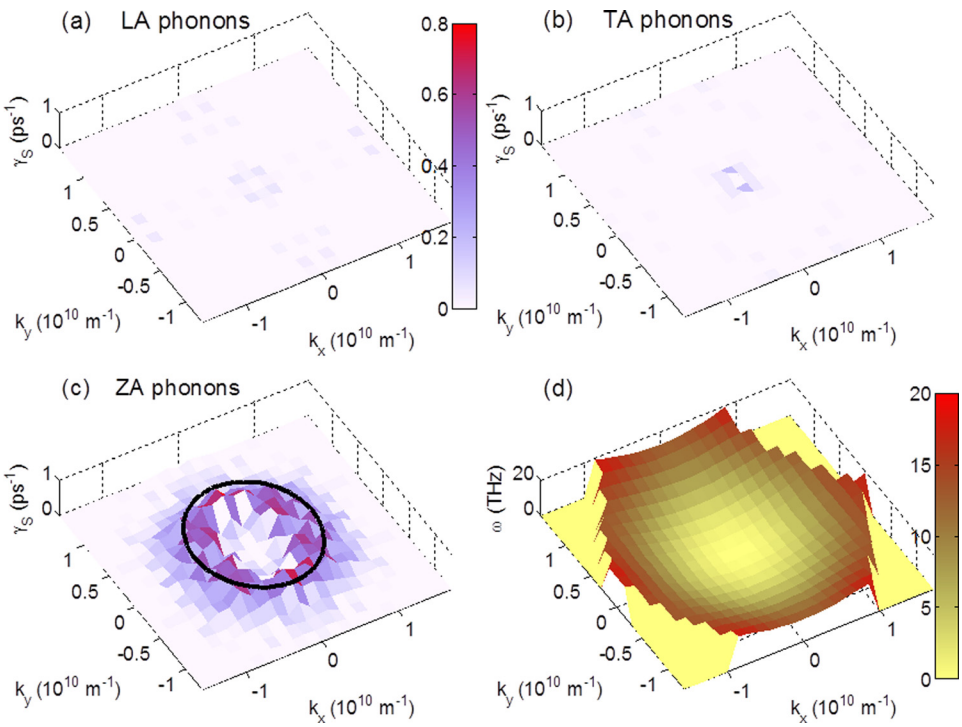

FIG. 3. Plot of the inelastic SLG-SiO_2 scattering rates γ_S for the (a) LA, (b) TA and (c) ZA phonons in the first Brillouin zone (BZ). The color bar for γ_S in ps^{-1} is shown in (a). We observe a band of ZA modes that dominate interfacial thermal transport, from 1.6 to 8.4 THz. The black circle of radius $7.7 \times 10^9\,\mathrm{m}^{-1} = 5.5\,\mathrm{THz}$ marks the region of peak scattering. (d) Plot of the ZA phonon frequency in the first BZ. The color bar for ω in THz is shown.

scattering event, we estimate the Kapitza conductance to be $h_{SED} \approx 16\ \mathrm{MW\ K^{-1}\,m^{-2}}$. This value is higher than h_{GK}, possibly because we overestimate the average fraction of energy transferred per scattering event or because of uncertainties in the estimation of γ_S.

In Figs. 3(a) and 3(b), the scattering rates of the LA and TA phonons are <0.1 ps^{-1} and do not show any discernible patterns, indicating that they couple very weakly with the substrate phonons. This occurs because they are polarized in the in-plane directions. On the other hand, in Fig. 3(c), the scattering rates of the ZA phonons show a significant peak between the center and the edge of the Brillouin zone [Fig. 3(d)], around $|\boldsymbol{k}| = 7.7 \times 10^9\,\mathrm{m}^{-1}$ (or $\omega = 5.5$ THz), as marked with the black circle. At the zone center, the γ_S is small. In other words, the long-wavelength ZA modes couple weakly with the substrate phonons. This agrees with our GK simulation results, which suggest that long-wavelength phonons do not contribute significantly to interfacial thermal transport, and that enlarging the domain size does not change the Kapitza conductance significantly. It also explains why the Kapitza conductance in related nanostructures like carbon nanotubes does not change significantly when the MD simulation domain is enlarged.[37] At the BZ edge, the γ_S is also small. We observe a "band" in the γ_S between the center and the edge, implying that there is a wave vector and a frequency selection rule in interfacial thermal transport mediated by ZA phonons. This band has a finite width from $\omega = 1.6$ to 8.4 THz, where $\gamma_S > 0.2$ ps^{-1} and the maximum scattering rates are up to ~ 0.8 ps^{-1}. A circle is drawn in Fig. 3(c) to indicate the position of the band.

In the continuum model of interfacial thermal transport in the graphene-on-SiO_2 system by Persson and co-workers,[14–16] it was proposed that the Kapitza conductance was dominated by the coupling between a single bending mode (in the graphene) and the Rayleigh mode in the substrate, because of wave vector and frequency conservation. However, due to surface roughness and other substrate imperfections, the coupling may not be strictly between the two modes, but "bands" of modes as a result of broadening. We believe that the plot of γ_S for ZA phonons in Fig. 3(c) lends weight to this model, despite the amorphous structure of the SiO_2 substrate and the atomistic nature of our simulations. The SED analysis supports the idea that a flexural resonance mechanism, as described by Persson and co-workers,[14–16] determines interfacial thermal transport. This is consistent with a recent spectral non-equilibrium MD work that shows that ZA modes are the most effective interfacial transport channel for graphene-3D substrate interfaces.

Given that only a restricted band of graphene ZA phonon modes ($\omega = 1.6$ to 8.4 THz or 6.6 to 34.7 meV) is involved in interfacial thermal transport, this implies that not all the ZA phonons, which are believed to dominate thermal conduction within the graphene,[40] are affected by scattering of the substrate surface phonons. The reduction in the thermal conductivity of supported graphene on a rough substrate has been found to be due primarily to the reduction in the lifetime of the sub-60 meV ($\omega < 14.5$ THz) ZA phonons.[7,40,41] Therefore, it may be possible to increase the lifetime of the ZA phonon modes and increase the thermal conductivity without affecting the Kapitza conductance by using a smoother substrate surface. The lifetime of the ZA phonon is affected by both static roughness scattering and dynamic scattering by the substrate vibrational modes. Our simulations indicate that most of the ZA phonon-phonon lifetime reduction is due to scattering by the former when the SLG is in contact with the substrate. Therefore, a smoother surface would reduce roughness scattering[42] without significantly affecting dynamic scattering by the substrate modes, which is necessary for interfacial heat dissipation in large graphene samples.

B. Non-equilibrium Green's function analysis

So far, our MD results suggest that a limited range of phonon ZA modes dominate interfacial thermal transport. However, these results are based on classical dynamics which obscure the quantum aspects of interfacial phonon transport. They also contain the effects of anharmonic interactions, and there are some numerical uncertainties in the line width estimation. In order to determine more precisely the dominant phonon modes in interfacial thermal transport, we compute the phonon transmittance $\Xi(\omega)$ across the SLG-SiO_2 interface as a function of the phonon frequency ω, using the non-equilibrium Green's function (NEGF) method[43] described in Appendix C. We plot the computed transmittance spectrum in Fig. 4(a), where dashed lines show results without the long wavelength correction (sharp distinct peaks appear due to the finite size of the domain) and solid lines show the long-wavelength correction. The plot shows that most of the transmission spectrum is dominated by sub-20 THz phonons. At low frequencies ($\omega < 10$ THz), the transmittance scales linearly with the frequency, i.e., $\Xi(\omega) \propto \omega$. This agrees with our SED result, which shows $\gamma_S \to 0$ at long wavelengths. We also compute and plot the polarization dependence of the transmission spectrum [in-plane-polarized (xy) vs. out-of-plane-polarized (z)] in Fig. 4(b). We find that the transmission spectrum is dominated by the z-polarized modes. Figure 4(c) shows the total, xy-polarized and z-polarized phonon density of states (PDOS). The sub-20 THz region corresponds to the flexural acoustic (ZA) phonon modes. A comparison of the transmission spectrum in Fig. 4(a) and the PDOS plot in Fig. 4(c) suggests that most of the Kapitza conductance is mediated by the ZA modes, confirming the SED analysis results.

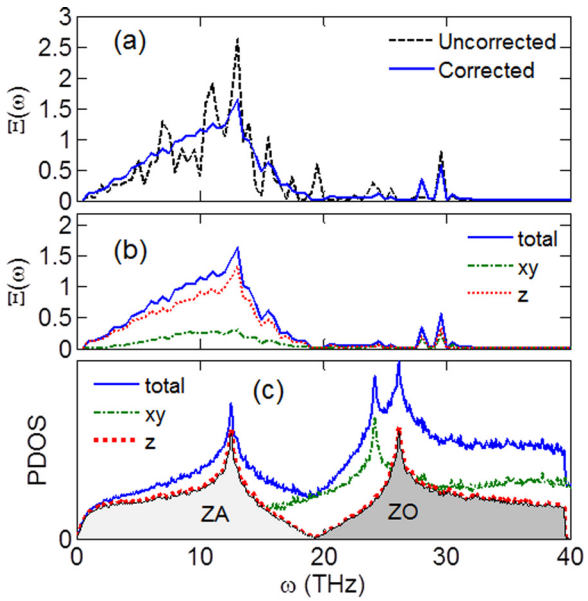

FIG. 4. NEGF simulation results of interfacial SLG-SiO_2 heat transfer. (a) The transmission spectrum with and without the long wavelength correction. Phonons with sub-20 THz frequencies dominate the interfacial thermal coupling. (b) The transmission spectrum resolved by polarization. (c) The phonon density of states (PDOS) resolved by polarization (xy for in-plane and z for out-of-plane). The flexural acoustic (ZA) and optical (ZO) parts of the out-of-plane PDOS are labeled and separated by the minimum at 19.4 THz.

Given the transmittance $\Xi(\omega)$ from the NEGF approach above, we calculate the Kapitza conductance h_{NEGF} with and without long-wavelength corrections over the given temperature range of 0 to 500 K as

$$h_{NEGF} = \frac{1}{2\pi A}\int_0^\infty \hbar\omega \frac{dN}{dT}\Xi(\omega)d\omega, \tag{4}$$

where N is the Bose-Einstein occupation factor and other quantities are as defined earlier. Figure 5(a) shows the temperature-dependent h_{NEGF} results and the corresponding high-temperature limit values of h_{NEGF} and h_{GK}. We find that there is no significant difference between the results with and without the long-wavelength corrections. This agrees well with our GK simulations in which the 4×-larger simulation domain gives only a slight difference in h_{GK} and supports the idea that long-wavelength modes do not contribute significantly to interfacial thermal transport. We also compare the classical limit of h_{NEGF} and h_{GK}. The results are in close agreement, suggesting that anharmonic effects and inelastic scattering[18,44] do not play an important role in interfacial thermal transport at room temperature (300 K) in the graphene-SiO_2 system. In the low temperature limit, we find that h_{NEGF} scales approximately as T^2, which follows from the approximate linear scaling of $\Xi(\omega)$ with ω (see Appendix D for a more detailed explanation). To gain insight into the polarization dependence of h_{NEGF}, we plot the xy- and z-polarized components of h_{NEGF} in Fig. 5(b). As expected from the transmission spectrum in Fig. 5(b), h_{NEGF} is dominated by the z-polarized modes although the xy-polarized modes do make a significant contribution. At 300 K, about 22% of the interfacial thermal conduction is due to in-plane-polarized modes, and 78% due to out-of-plane (ZA) modes.

The dominant role of the ZA modes in mediating interfacial phonon transport implies that the dispersion of the flexural phonons is important. If the bending stiffness of the

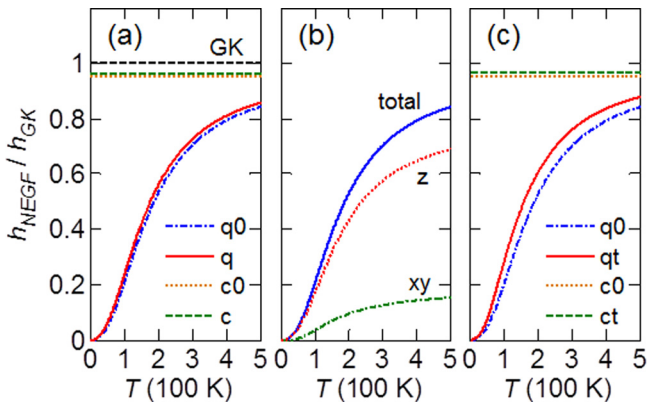

FIG. 5. NEGF results of the Kapitza conductance normalized by the Green-Kubo value, h_{NEGF}/h_{GK}, where $h_{GK} = 10.3$ MW $K^{-1}m^{-2}$. (a) Temperature dependence of h_{NEGF} with ("q") and without ("q0") long-wavelength correction. The corresponding classical h_{NEGF} values with ("c") and without ("c0") long-wavelength are also plotted. (b) The Kapitza conductance resolved by polarization ("xy" for in-plane, "z" for out-of-plane, and "total" for all polarizations) at different temperatures. (c) Temperature dependence of h_{NEGF} using the Lindsay-Broido parameters[31] ("q0") and the original Tersoff parameters[45] ("qt"). The corresponding classical h_{NEGF} values using the Lindsay-Broido parameters ("c0") and the original Tersoff parameters ("ct") are also shown.

graphene is decreased, the resultant frequencies and group velocities of the flexural phonons are smaller. To see the consequence of the decreased bending stiffness for interfacial phonon transport, we also use the original Tersoff potential for carbon[45,46] instead of the optimized Tersoff potential parameters of Lindsay and Broido.[31] The original Tersoff parameters give a smaller bending stiffness[31] and hence, lower frequencies and group velocities for the ZA modes. We plot the corresponding h_{NEGF} values in Fig. 5(c). The h_{NEGF} values for the original Tersoff parameters are slightly larger because the lower frequencies imply a higher Bose-Einstein occupation at finite temperatures. The ZA modes contribute about 83% of the total conductance at 300 K. In the high-temperature or classical limit, the difference in h_{NEGF} is smaller because the higher-frequency modes are all occupied. The original Tersoff parameters still yield a higher h_{NEGF}, possibly because the reduced bending stiffness makes graphene more flexible and improves its conformance to the substrate surface.

IV. CONCLUSIONS

In summary, we have studied the Kapitza conductance of the SLG-SiO_2 interface in SiO_2-supported SLG with atomistic MD simulations, using the Green-Kubo, spectral energy density and non-equilibrium Green's function methods. The classical and quantum mechanical Kapitza conductance are computed to be $h_K \approx 10$ to 16 and 7.2 MW $K^{-1} m^{-2}$ at 300 K, respectively, consistent with the existing experimental observations. Our GK results converge with the high-temperature NEGF results, suggesting that anharmonic and multi-phonon effects are insignificant at room temperature. The GK and NEGF results also suggest that the simulation domain size does not significantly affect the Kapitza conductance. We do not find a significant change in the Kapitza conductance when a different interatomic potential for the C atoms is used.

We have also determined the main phonons in interfacial thermal transport. The SED analysis of the phonon lifetimes shows that a restricted band of ZA phonon modes ($\omega = 1.6$ to 8.4 THz) dominates the lattice Kapitza conductance and supports the continuum model of flexural resonance suggested by Persson and co-workers. This is supported by our NEGF calculations which also show that the Kapitza conductance is dominated by the ZA phonons. The low-temperature Kapitza conductance is determined to scale as $\sim T^2$ due to the linear ω-dependence of the phonon transmittance at low frequencies. Our analysis sheds light on the microscopic mechanism of interfacial heat dissipation which can be exploited for the thermal management of 2D devices.

ACKNOWLEDGMENTS

We acknowledge partial support from the National Science Foundation (NSF) EFRI 2-DARE Grant No. 1542883, the NSF DMREF Grant No. 1534279, the NSF Center for Power Optimization of Electro-Thermal Systems (POETS), and the Air Force Office of Scientific Research (AFOSR) Grant Nos. FA9550-12-1-0037 and FA9550-14-1-0251. Z.Y.O. also acknowledges support from the Agency for Science, Technology and Research (A*STAR), Singapore.

APPENDIX A: GREEN-KUBO METHOD IN MD SIMULATIONS

We use the GK method in equilibrium MD simulations,[23,35,36] first developed in the paper[35] by Ong and Pop, to compute the linear *classical* Kapitza conductance. The Kapitza conductance (h_{GK}) can be computed using the Green-Kubo relation formula

$$h_{GK} = \lim_{t\to\infty} h(t) = \lim_{t\to\infty} \frac{1}{Ak_BT^2} \int_0^t d\tau \, \langle Q(\tau)Q(0)\rangle, \qquad \text{(A1)}$$

where A, k_B, T and Q are the interfacial area, the Boltzmann constant, the classical temperature and the interfacial heat flux, respectively; $h(t)$ is the finite integral of the auto-correlation of Q. In our simulations at equilibrium, the instantaneous interfacial heat flux is recorded over 1 ns, the maximum duration over which energy drift in the MD simulations is manageable, at intervals of 5 fs. Given the finite duration of our simulation, we take the average of $h(t)$ between $t = 20$ and 40 ps to estimate h_{GK}. In our GK calculations, we average over the 5 independent substrates and 6 sets of initial conditions for each substrate. Hence, a total of 30 independent runs is used to compute h_{GK}.

An advantage of using the GK method is that it automatically incorporates anharmonic and possible multi-phonon effects.[44] Also, the calculated Kapitza conductance h_{GK} is strictly a linear response coefficient. However, because it is computed from the fluctuation of the classical interfacial heat flux, h_{GK} does not contain quantum effects that are important at low temperatures. Therefore, we need to use other methods to compute the Kapitza conductance at low temperatures. Another disadvantage of the GK method is that it is limited by the system and interfacial size. It is not possible to include the contributions from longer-wavelength modes without enlarging the simulation domain and incurring greater computational expense.

APPENDIX B: SPECTRAL ENERGY DENSITY (SED) ANALYSIS

A different understanding of the thermal transport process can be obtained by treating and studying the SLG as a dissipative system.[47] As SLG consists of a single layer of carbon atoms, its phonon modes are directly coupled to the phonon modes of the substrate, which we can act as a reservoir because it has many more degrees of freedom than the SLG. This coupling has a dissipative effect on the motion of the SLG atoms, which can be analyzed using the phonon spectral energy density (SED) method.[23,25]

The SED method for phonon relaxation time extraction from MD simulations has been used for a range of materials.[23–26,48] A detailed description of our SED method can be found in Ref. 25 and its supplement. The time steps for the suspended and supported SLG simulations are chosen to be 0.8 and 0.2 fs, respectively, to ensure stability and resolution of all possible vibrational frequencies. Starting from pre-optimized geometries, after initial equilibration at constant volume and temperature (NVT), the systems are run in the constant volume and energy ensemble (NVE), from which

the atomic velocities are extracted and post-processed. The phonon properties are found to converge with simulation durations of 3.2 and 1.0 ns in the NVE ensemble for the suspended and supported SLG, respectively. The phonon SED technique converts the trajectories of the SLG atoms into the energy density spectra of various phonon modes with different polarizations, wave vectors and frequencies. The relaxation time of different phonon modes can then be extracted from their line widths.

Here, we are not interested in the relaxation time *per se* but to the *change* in the relaxation time that we can attribute to inelastic scattering. We assume that only three *independent* mechanisms contribute to the SLG phonon lifetime in our MD simulations:[23]

1. Anharmonic coupling between SLG phonon modes (γ_U)
2. Interfacial scattering by static vdW bonds at the interface (γ_B)
3. Inelastic SLG-SiO_2 phonon-phonon scattering (γ_S)

In the context of interfacial thermal transport, the third mechanism is the most important because it results in energy exchange between the SLG and the substrate. The first mechanism is inelastic but does not change the total energy of the SLG modes since it affects only the energy redistribution between the SLG modes. The second mechanism corresponds to elastic scattering and thus does not affect the energy of the scattered SLG modes.

If we assume that these processes are independent, we can write the inverse phonon lifetime as the sum of their scattering rates, i.e.,

$$\gamma = \gamma_U + \gamma_B + \gamma_S. \tag{B1}$$

In particular, we are interested in γ_S, which we assume to be responsible for energy exchange between the SLG and the substrate. As all three processes contribute to the phonon lifetime, we need to modify the simulation conditions to isolate γ_S. To do that, two different sets of MD simulations are performed. In the first set (γ_{Froz}), we freeze the atoms of the substrate but allow the graphene atoms to move freely. The frozen substrate implies that there is no SLG-SiO_2 phonon-phonon scattering, so that $\gamma_{Froz} = \gamma_U + \gamma_B$. In the second set ($\gamma_{Vibr}$), the substrate atoms are allowed to vibrate. Thus, $\gamma_{Vibr} = \gamma_U + \gamma_B + \gamma_S$. The difference between γ_{Froz} and γ_{Vibr} yields the SLG-SiO_2 phonon-phonon scattering rate (γ_S).

It must be mentioned that underlying our procedure of modifying the simulation conditions to isolate the individual scattering rates is the assumption that the scattering rates γ_U, γ_B and γ_S are not significantly altered by these modifications. This assumption should hold provided that the SLG-SiO_2 interaction is sufficiently weak. However, this "sufficiently weak" assumption can only be justified post hoc from our simulation results and analyses, as will be shown below.

The SLG-SiO_2 Kapitza conductance estimated from the SED analysis (h_{SED}) can then be written as

$$h_{SED} = \frac{1}{A}\sum_{k_x}\sum_{k_y}\sum_{\beta} \xi\hbar\omega(k_x,k_y,\beta)\gamma_S(k_x,k_y,\beta)\frac{dN(k_x,k_y,\beta)}{dT}, \tag{B2}$$

where k_x and k_y are the x and y components of the wave vector and β indexes the polarization (LA, LO, TA, TO, ZA or ZO). The variables A, ξ, $\hbar$, ω and N represent the interfacial area, the average fraction of energy lost per scattering event, the Planck constant, the phonon frequency and the Bose-Einstein occupation factor, respectively. We assume $\xi \approx 0.5$, i.e., 50% of the energy is lost in each scattering event, although the percentage of energy dissipated by each mode should in principle depend on the frequency, the wavelength and the polarization. In addition, it should also be noted that γ_S, the SLG-SiO_2 phonon-phonon scattering rate, depends implicitly on the thermodynamic distribution of the substrate phonons which can be affected by quantum effects that are not captured in our classical MD simulations. This may affect the accuracy of Eq. (B2), as the lower occupation of SiO_2 phonon modes at higher frequencies should lower γ_S and the overall conductance. In the high-temperature limit, Eq. (B2) yields

$$h_{SED} = \frac{\xi k_B}{A}\sum_{k_x}\sum_{k_y}\sum_{\beta}\gamma_S(k_x,k_y,\beta). \tag{B3}$$

The contribution from each mode is $h(k_x,k_y,\beta) = (\xi k_B/A)\,\gamma_S(k_x,k_y,\beta)$.

APPENDIX C: NON-EQUILIBRIUM GREEN'S FUNCTION

Given the limitations of the GK method, we use a modified version of the NEGF method for phonon transport,[43] an intrinsically quantum mechanical technique, to calculate the temperature dependence of the Kapitza conductance as well as to distinguish the contributions from the in-plane and out-of-plane modes. The method can also be modified to take into account long wavelength contributions. However, because it assumes only harmonic interaction within and between the lattices, it does not contain any explicit anharmonic or multi-phonon effects. This does not matter at low temperatures, relative to the Debye temperature of SiO_2 ($\Theta_D = 470$ K),[49] or if we expect anharmonic effects to be small. At higher temperatures (relative to Θ_D) where anharmonic effects may be important, we can safely employ the GK result.

The thermal conductance h_{NEGF} is given by

$$h_{NEGF} = \frac{1}{2\pi A}\int_0^{\infty}\hbar\omega\frac{dN}{dT}\Xi(\omega)d\omega, \tag{C1}$$

where N is the Bose-Einstein occupation and $\Xi(\omega)$ is the transmission factor. The transmission factor is given by[43]

$$\Xi(\omega) = 4\pi^2 Tr\left[\rho_G(\omega)D_G^A(\omega)k_{GS}\rho_S(\omega)D_S^R(\omega)k_{SG}\right], \tag{C2}$$

where

$$\rho_{G,S} = \frac{1}{2\pi}\left(G_{G,S} - G_{G,S}^{\dagger}\right), \tag{C3}$$

is the density matrix of the graphene (G) or substrate (S) lattice. We define

$$D_G^A = \left(I - K_{GS}G_S^\dagger K_{SG}G_G^\dagger\right)^{-1}, \qquad D_S^R = \left(I - K_{SG}G_G K_{GS}G_S\right)^{-1}, \tag{C4}$$

where G_G (G_S) is the Green's function for the graphene (substrate) lattice, and is given by

$$G_{S,G}(\omega) = \left[\omega^2 + i\gamma(\omega)\omega - K_{S,G}\right]^{-1}, \tag{C5}$$

where $\gamma(\omega)$ represents the phenomenological frequency-dependent dissipative rate which we set as $\gamma(\omega) = 0.01\omega$. The matrices K_S, K_G, K_{SG} and K_{GS} are the sub-matrices of the force constant matrix K, i.e.,

$$K = \begin{pmatrix} K_G & K_{GS} \\ K_{SG} & K_S \end{pmatrix}, \tag{C6}$$

where its elements are given by

$$K_{ij} = \frac{1}{(m_i m_j)^{1/2}} \frac{\partial^2 E}{\partial u_i \partial u_j}, \tag{C7}$$

where E is the interatomic potential, u_i is the i-th degree of freedom, and m_i is the corresponding atomic mass. The matrix K is calculated using the General Lattice Utility Program (GULP) code.[30] The classical limit of h_{NEGF} in Eq. (C1) can be obtained by setting $T \to \infty$ and replacing $\hbar\omega(\partial N/\partial T)$ with the Boltzmann constant k_B.

The NEGF method, as presented so far, suffers from the same size limitation as the GK method. Given that the length (L_x) and the width (L_y) of the simulated graphene-SiO_2 system are 4.4 and 4.3 nm, respectively, longer wavelength modes are not included in the calculation. However, assuming that the interatomic potential cutoff distance is less than half of the domain size, this can be remedied by treating the simulation domain as a supercell, and then modifying Eq. (C7), i.e.,

$$K_{ij} = \frac{\partial^2 E}{\partial u_i \partial u_j} \to K_{ij}(k_x, k_y) = \frac{\partial^2 E}{\partial u_i \partial u_j} \exp\left[i(k_x L_{x,ij} + k_y L_{y,ij})\right], \tag{C8}$$

where

$$L_{x,ij} = \begin{cases} L_x & \text{if} \quad 2x_{ij} > L_x \\ 0 & \text{if} \quad -L_x < 2x_{ij} \le L_x \\ -L_x & \text{if} \quad 2x_{ij} \le -L_x, \end{cases} \tag{C9}$$

and x_{ij} is the x-directional equilibrium atomic distance between the i-th and j-th degrees of freedom. $L_{y,ij}$ is similarly defined. The variables k_x and k_y are the wave vectors associated with the translational periodicity in the x and y-directions, and are given by $0 \le k_x < 2\pi/L_x$ and $0 \le k_y < 2\pi/L_y$, respectively. The contribution from the longer wavelength modes can be included by computing the transmission factor for each pair of (k_x,k_y) and then averaging over all possible (k_x,k_y) values. In our calculations, we approximate the (k_x,k_y)-space average with a grid of 10×10 points.

APPENDIX D: T^2 DEPENDENCE OF h_{NEGF}

At low temperatures, the Bose-Einstein occupation factor N can be approximated as

$$\lim_{T\to 0} N = e^{-\frac{\hbar\omega}{k_B T}}. \tag{D1}$$

So, the expression for h_{NEGF} becomes

$$h_{NEGF} = \frac{k_B}{2\pi A}\int_0^\infty \left(\frac{\hbar\omega}{k_B T}\right)^2 e^{-\frac{\hbar\omega}{k_B T}} \Xi(\omega) d\omega. \tag{D2}$$

If we assume that $\Xi(\omega) \propto \omega$ for $\omega \ll k_B T/\hbar$, then $h_{NEGF} \propto T^2$.

[1] A. Behnam, A. S. Lyons, M.-H. Bae, E. K. Chow, S. Islam, C. M. Neumann, and E. Pop, Nano Lett. **12**(9), 4424–4430 (2012).
[2] R.-H. Kim, M.-H. Bae, D. G. Kim, H. Cheng, B. H. Kim, D.-H. Kim, M. Li, J. Wu, F. Du, H.-S. Kim, S. Kim, D. Estrada, S. W. Hong, Y. Huang, E. Pop, and J. A. Rogers, Nano Lett. **11**(9), 3881–3886 (2011).
[3] Y.-M. Lin, K. A. Jenkins, A. Valdes-Garcia, J. P. Small, D. B. Farmer, and P. Avouris, Nano Lett. **9**(1), 422–426 (2008).
[4] Y. Wu, K. A. Jenkins, A. Valdes-Garcia, D. B. Farmer, Y. Zhu, A. A. Bol, C. Dimitrakopoulos, W. Zhu, F. Xia, P. Avouris, and Y.-M. Lin, Nano Lett. **12**(6), 3062–3067 (2012).
[5] M.-H. Bae, S. Islam, V. E. Dorgan, and E. Pop, ACS Nano **5**(10), 7936–7944 (2011).
[6] S. Islam, L. Zuanyi, V. E. Dorgan, B. Myung-Ho, and E. Pop, IEEE Electron Device Lett. **34**(2), 166–168 (2013).
[7] M.-H. Bae, Z. Li, Z. Aksamija, P. N. Martin, F. Xiong, Z.-Y. Ong, I. Knezevic, and E. Pop, Nat Commun. **4**, 1734 (2013).
[8] E. Pop, V. Varshney, and A. K. Roy, MRS Bull. **37**(12), 1273–1281 (2012).
[9] S. Fratini and F. Guinea, Phys. Rev. B **77**(19), 195415 (2008).
[10] Z.-Y. Ong and M. V. Fischetti, Phys. Rev. B **86**, 165422 (2012).
[11] J. K. Viljas and T. T. Heikkila, Phys. Rev. B **81**(24), 245404 (2010).
[12] T. Low, V. Perebeinos, R. Kim, M. Freitag, and P. Avouris, Phys. Rev. B **86**(4), 045413 (2012).
[13] Z.-Y. Ong, M. V. Fischetti, A. Y. Serov, and E. Pop, Phys. Rev. B **87**(19), 195404 (2013).
[14] B. N. J. Persson and H. Ueba, J. Phys.: Condens. Matter **22**(46), 462201 (2010).
[15] B. N. J. Persson and H. Ueba, Europhys. Lett. **91**(5), 56001 (2010).
[16] B. N. J. Persson, A. I. Volokitin, and H. Ueba, J. Phys.: Condens. Matter **23**(4), 045009 (2011).
[17] E. T. Swartz and R. O. Pohl, Rev. Mod. Phys. **61**(3), 605–668 (1989).
[18] J. C. Duda, P. E. Hopkins, T. E. Beechem, J. L. Smoyer, and P. M. Norris, Superlattices Microstruct. **47**(4), 550–555 (2010).
[19] S.-W. Chang, A. K. Nair, and M. J. Buehler, J. Phys.: Condens. Matter **24**(24), 245301 (2012).
[20] L. Hu, T. Desai, and P. Keblinski, Phys. Rev. B **83**(19), 195423 (2011).
[21] Z.-Y. Ong, Y. Cai, and G. Zhang, Phys. Rev. B **94**(16), 165427 (2016).
[22] K. F. Mak, C. H. Lui, and T. F. Heinz, Appl. Phys. Lett. **97**(22), 221904 (2010).
[23] Z.-Y. Ong, E. Pop, and J. Shiomi, Phys. Rev. B **84**(16), 165418 (2011).
[24] B. Qiu, H. Bao, G. Zhang, Y. Wu, and X. Ruan, Comput. Mater. Sci. **53**(1), 278–285 (2012).
[25] B. Qiu and X. Ruan, Appl. Phys. Lett. **100**(19), 193101–193104 (2012).
[26] J. A. Thomas, J. E. Turney, R. M. Iutzi, C. H. Amon, and A. J. H. McGaughey, Phys. Rev. B **81**(8), 081411 (2010).
[27] M. Freitag, M. Steiner, Y. Martin, V. Perebeinos, Z. Chen, J. C. Tsang, and P. Avouris, Nano Lett. **9**(5), 1883–1888 (2009).
[28] Z. Chen, W. Jang, W. Bao, C. N. Lau, and C. Dames, Appl. Phys. Lett. **95**(16), 161910 (2009).
[29] S. Plimpton, J. Comput. Phys. **117**(1), 1–19 (1995).
[30] J. D. Gale and A. L. Rohl, Mol. Simul. **29**(5), 291–341 (2003).
[31] L. Lindsay and D. A. Broido, Phys. Rev. B **81**(20), 205441 (2010).
[32] S. Munetoh, T. Motooka, K. Moriguchi, and A. Shintani, Comput. Mater. Sci. **39**(2), 334–339 (2007).
[33] S. P. Koenig, N. G. Boddeti, M. L. Dunn, and J. S. Bunch, Nat. Nanotechnol. **6**(9), 543–546 (2011).
[34] J. Hu, X. Ruan, and Y. P. Chen, Nano Lett. **9**(7), 2730–2735 (2009).

[35]Z.-Y. Ong and E. Pop, J. Appl. Phys. **108**(10), 103502–103508 (2010).
[36]Y. Chalopin, K. Esfarjani, A. Henry, S. Volz, and G. Chen, Phys. Rev. B **85**(19), 195302 (2012).
[37]C. F. Carlborg, J. Shiomi, and S. Maruyama, Phys. Rev. B **78**(20), 205406 (2008).
[38]Z. Xu and M. J. Buehler, J. Phys.: Condens. Matter **24**(47), 475305 (2012).
[39]Z.-Y. Ong and E. Pop, Phys. Rev. B **84**(7), 075471 (2011).
[40]J. H. Seol, I. Jo, A. L. Moore, L. Lindsay, Z. H. Aitken, M. T. Pettes, X. Li, Z. Yao, R. Huang, D. Broido, N. Mingo, R. S. Ruoff, and L. Shi, Science **328**(5975), 213–216 (2010).
[41]L. Lindsay, D. A. Broido, and N. Mingo, Phys. Rev. B **82**(11), 115427 (2010).
[42]Z. Aksamija and I. Knezevic, Phys. Rev. B **86**(16), 165426 (2012).
[43]N. Mingo "Green's Function Methods for Phonon Transport Through Nano-Contacts," in *Thermal Nanosystems and Nanomaterials*, edited by S. Volz (Springer-Verlag Berlin, 2009), p. 63.
[44]P. E. Hopkins, J. Appl. Phys. **106**(1), 013528 (2009).
[45]J. Tersoff, Phys. Rev. Lett. **61**(25), 2879–2882 (1988).
[46]J. Tersoff, Phys. Rev. B **37**(12), 6991–7000 (1988).
[47]D. J. Diestler and R. S. Wilson, J. Chem. Phys. **62**(4), 1572–1578 (1975).
[48]N. de Koker, Phys. Rev. Lett. **103**(12), 125902 (2009).
[49]H. Wang, Y. Xu, M. Shimono, Y. Tanaka, and M. Yamazaki, Mater. Trans. **48**(9), 2349–2352 (2007).